ACME2: An Extended Toolbox for Automated Cirque Metrics Extraction

Yingkui Li[a*], Ian S. Evans[b], Matteo Spagnolo[c], Ramón Pellitero[d], Iestyn D. Barr[e], Jeremy C. Ely[f]

[a] Department of Geography & Sustainability, University of Tennessee, Knoxville, TN 37996, USA

[*] Corresponding author. Email address: yli32@utk.edu (Y. Li).

[b] Department of Geography, University of Durham, Durham, UK, DH1 3LE, UK

[c] Department of Geography and the Environment, School of Geosciences, University of Aberdeen, UK

[d] Departamento de Geografía, Universidad Nacional de Educación a Distancia (UNED), Madrid, Spain

[e] Department of Natural Sciences, Manchester Metropolitan University, Manchester, UK

[f] Department of Geography, University of Sheffield, UK

Abstract: With the availability of improved digital elevation models (DEMs) of global coverage, the morphological analysis of large populations of glacial cirques is possible, and can be used to derive important palaeoclimate and environmental information related to the distribution and history of former glaciers. In 2017, an ArcGIS toolbox, ACME (Automated Cirque Metrics Extraction), was developed to derive 16 cirque metrics based on input cirque outlines, threshold midpoints and DEMs. ACME has been widely used in cirque morphological analysis and regional comparisons. This paper presents a revised and extended toolbox, ACME2. This extended toolbox includes new functions to automatically derive cirque threshold midpoints (cirque foci) and 49 morphometric and locational variables, with attributes related to cirque location, size, shape, altitude, slope, and aspect, including variables related to the median axis, as well as 3 input metadata attributes. ACME2 also improves the methods for calculation of the hypsometric maximum and integral, and implements a new method for plan closure to be more consistent with the original definition. All ACME2 tools are coded in Python and can be imported into ArcGIS with user-friendly interfaces. Comparisons for 155 cirques in the English Lake District and 51 in the Shulaps Range, British Columbia, indicate consistency between the ACME2-derived and manually derived metrics, with most correlations $r > 0.90$: none <0.70. ACME2 provides more cirque metrics and automates the whole calculation sequence with cirque outlines and DEMs. Its comprehensive approach facilitates understanding of cirque form and development in all its variety.

Keywords: cirques; morphometric analysis; palaeoclimate; ACME; ACME2

1. Introduction

Cirques are a typical erosional landform formed by relatively small glaciers primarily during the initiation and termination of glaciations (e.g. Gardner, 1987; Evans and Cox, 1995; Sanders et al., 2012; Evans, 2021). The presence of cirques is a long-lasting indicator of past glaciation, so cirque morphology has been used to infer palaeoclimate and environmental conditions such as solar radiation, cloud cover, wind direction, and the magnitude of past glaciations (Nelson and Jackson, 2002; Evans, 1977, 2006; Mîndrescu et al., 2010; Barr and Spagnolo, 2015; Oien et al., 2020, 2022; Li et al., 2023; Barr et al., 2023). Cirques have also been used as evidence of the role of glacial erosion in limiting mountain heights, commonly referred to as the "glacial buzzsaw" hypothesis (Brozović et al., 1997; Mitchell and Montgomery, 2006; Egholm et al., 2009; Mîndrescu and Evans, 2014).

Built on earlier lists of cirque attributes such as in Andrews and Dugdale (1971), Evans and Cox (1995) defined a series of morphometric and contextual descriptors of cirques to provide full support for the identification of cirques, to assess controls of cirque size, shape, and location, and to demonstrate patterns in cirque development. Specifically, this series of morphometric and contextual descriptors included 23 separately measured or estimated variables and 6 further variables calculated from those. Of the 23, 17 are on ratio scales, two on circular scales, two ordinal, and two nominal classifications. All but the last four were measured from contour maps.

Advances in Geographic Information Systems (GIS) and remote sensing (RS) techniques and the availability of Digital Elevation Models (DEMs) of global coverage (Anders et al., 2010; Principato and Lee, 2014; Li and Zhao, 2022) have allowed for the morphological analysis of large cirque datasets to reconstruct palaeoclimate and environmental conditions and to test the buzzsaw hypothesis (Barr and Spagnolo, 2015; Mitchell and Humphries, 2015; Evans and Cox, 2017; Zhang et al., 2020; Li et al., 2023). An ArcGIS toolbox, ACME (Automated Cirque Metric Extraction) was developed by Spagnolo et al. (2017) to derive 16 morphological metrics, including length, width, circularity, planar and three-dimensional (3D) area, elevation, slope, aspect, plan closure, and hypsometry. This requires three inputs: cirque outlines (polygons), threshold midpoints, and a DEM. This toolbox has been used to extract cirque metrics and infer palaeoclimate conditions in various settings worldwide, including: Britain and Ireland (Barr et al., 2017, 2019), the Guadarrama and Somosierra mountains in Spain (Pedraza et al., 2019), the Faeroe Islands (Wallick and Principato, 2020), High Mountain Asia (Zhang et al., 2020, 2021; Li et al., 2022; Li et al., 2023), and Antarctica (Barr et al., 2022, 2023). Use of DEMs allowed

ACME to calculate new descriptors such as hypsometric integral, mean slope and 3D area.

However, it has become clear that some modifications and extensions to ACME are desirable. First, the 16 metrics derived by ACME do not include all metrics proposed by Evans and Cox (1995): in particular, they omit the axis-related metrics and relevant contextual metrics outside the cirque outlines, such as the maximum elevation above the cirque, which are useful in explaining how a cirque developed. Second, the calculation method of plan closure in ACME produces results that are not comparable to those from the manual approach of Evans and Cox (1995) (Section 2.3). Without judging which is to be preferred, it is useful to have results that can be compared with those in earlier literature. Third, some ACME metric calculations are not computationally optimal. For example, ACME-derived hypsometric maximum and integral require the specification of a class width for altitude analysis, which makes the metrics sensitive to that potentially arbitrary choice. Finally, and more importantly, ACME requires the input of cirque outlines and threshold midpoints for the calculation. Both these features are traditionally based on manual digitization. Li and Zhao (2022) developed an ArcGIS toolbox, AutoCirque, to automatically delineate cirque outlines from DEMs, partially resolving the need to automate digitization. However, cirque threshold midpoints are still based on manual digitization, which could be perceived as somewhat subjective and, being time-consuming, might hinder the morphometric analysis of large cirque datasets for regional comparisons.

In this paper, we present a revised and extended ACME toolbox, ACME2. This extended toolbox adds functions to automatically derive cirque threshold midpoints (foci), extract 49 metrics related to cirque location, size, shape, altitude, slope, aspect, including axis-related variables, and records 3 input metadata variables. ACME2 also improves methods for the hypsometric maximum and integral calculations and develops a new plan closure calculation method that is more consistent with manually derived values. All ACME2 tools are coded in Python (open source) and are designed to be easily imported into ArcGIS with user-friendly interfaces. The results are calibrated and validated against manual methods. This updated toolbox allows for the rapid and automated analysis of large cirque datasets for palaeoclimate reconstruction and regional comparisons.

2. Methodology

2.1 Input datasets

ACME2 requires two input datasets to work: a DEM and a cirque outline (polygon) file. Cirque outlines are typically digitized manually from topographic maps, aerial photographs, satellite images, and DEMs (e.g. Evans and Cox, 1995; Federici and Spagnolo, 2004; Seif and Ebrahimi, 2014). In recent years, object-based image classification, deep learning, and automated approaches have been developed to help identify and map cirque outlines (Eisank et al., 2010; Anders et al., 2015; Li and Zhao, 2022; Scuderi and Nagle-McNaughton, 2022).

Both datasets need to have the same projected coordinate system (a UTM or a national grid) to ensure the correct calculations. If one of the projections is in the geographic coordinate system (GCS) of degrees of latitudes and longitudes, or if the two projections are different from each other, a warning is displayed and the tools will not operate.

2.2 Cirque focus or threshold midpoint delineation

Many cirque-related metrics, such as axis aspect, length, width, and their related variables, require the input of a cirque threshold midpoint (the ‘focus’ of Evans and Cox, 1995) for their calculation. The cirque threshold is a relatively flat part of the cirque outline at the valley bottom, although it includes minor topographic variations. In ACME2, we provide two new automated methods to derive the threshold foci, although users can still provide their own digitized points.

The first method assumes that the intersection point between the cirque outline and the mainstream flowing out of the cirque is likely to be close to the cirque focus, although it is sometimes at one side of the cirque threshold. This approach is called ‘mainstream exit’ in ACME2. A set of hydrological tools are required to derive this point, including filling sinks of the DEM, flow direction, and flow accumulation. The intersection point between the cirque outline and the mainstream corresponds to the highest flow accumulation point within the cirque outline. Fig. 1 illustrates the flowchart of the mainstream exit approach to derive the threshold foci.

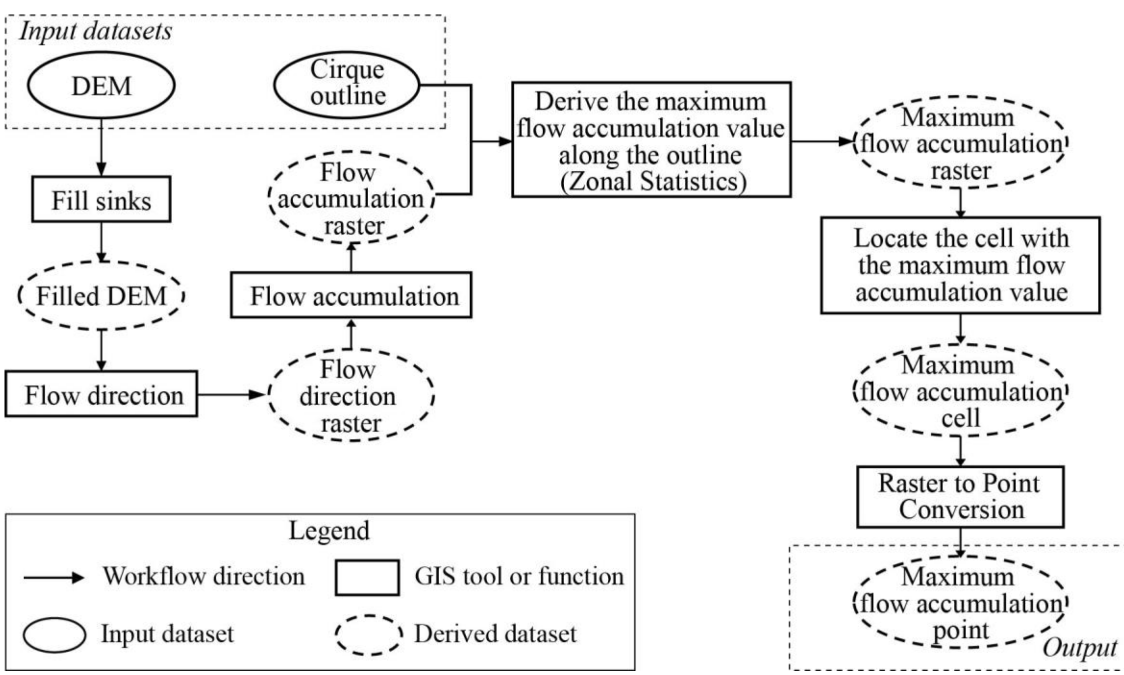

Fig. 1 The flowchart of the mainstream exit approach to derive the threshold foci.

The second method, named the threshold midpoint approach, attempts to derive the middle point of the cirque threshold as the focus. First, the cirque outline is divided in two halves using the mid-range elevation along the cirque outline (Fig. 2a). The higher part mainly includes the crest and ridge lines. The lower part includes the cirque threshold, valley sides, and maybe some ridge lines. Because the cirque threshold is relatively flat compared to sidewalls, it corresponds to the highest peak on the frequency distribution (histogram) of the elevations along the low part of the outline (Fig. 2b). We add one elevation bin (5 meters) to this highest frequency elevation to account for the potential high grounds on the cirque threshold and use it as a cutoff elevation to determine the cirque threshold section (Fig. 2c). This excludes both cirque sidewalls. If the low part of the cirque outline is divided into multiple segments by this elevation, segments with small gaps (less than 60 m or the length of the smallest segment) are connected in order to remove the impact of small and isolated high grounds on the cirque threshold. If multiple segments still exist after that, only the longest segment is kept, to remove potential isolated short segments of the cirque outline, which are far away from the threshold but lower than the derived cutoff elevation. Finally, the middle point of the extracted cirque threshold is determined as the threshold focus of the cirque (Fig. 2d).

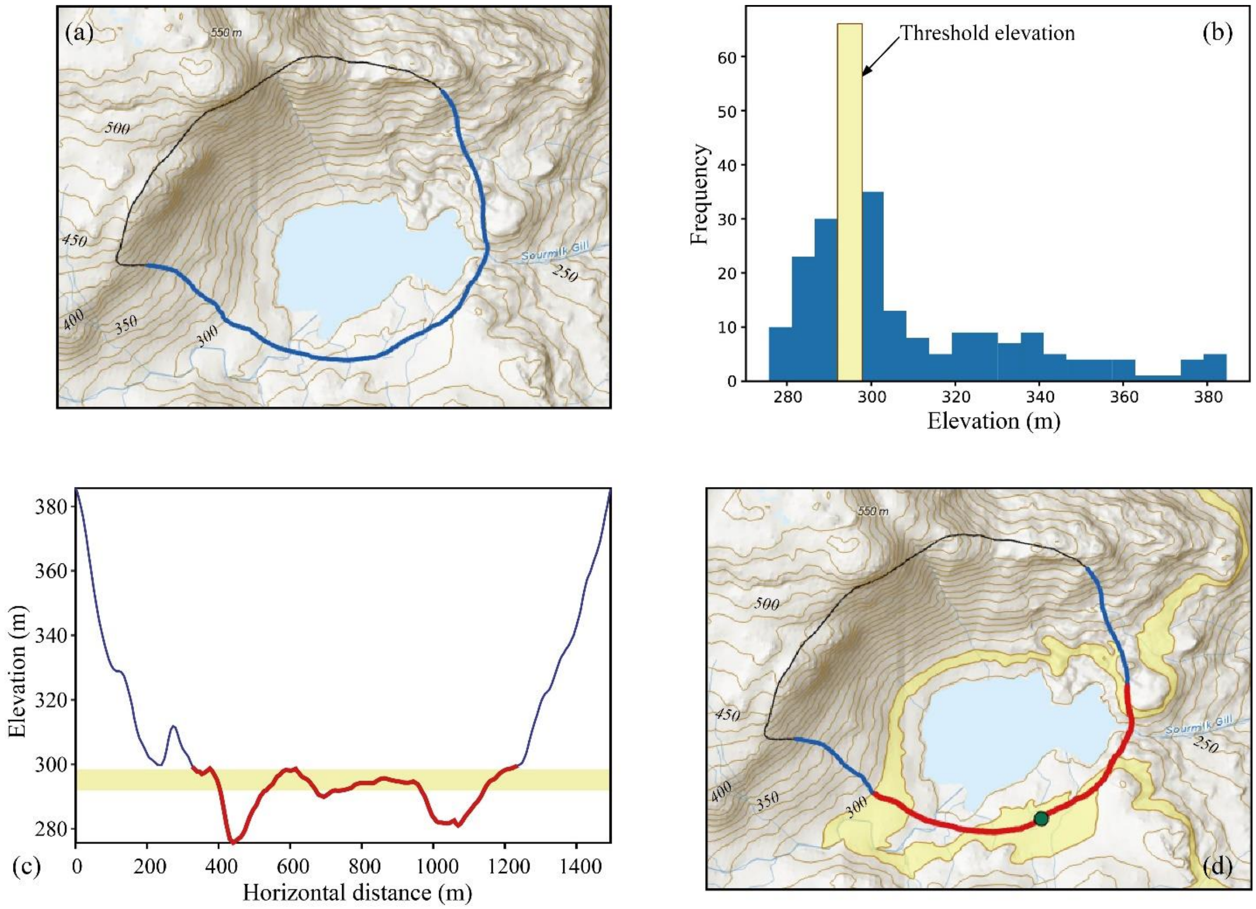

Fig. 2 The general steps to derive the cirque threshold focus point. (a) The lower half of the cirque outline (blue line), below the mid-range of elevations along the cirque outline. (b) The frequency distribution (histogram) of elevations on the lower half of the cirque outline. The highest peak (yellow) corresponds to the modal elevation of the cirque threshold. (c) The topographic profile of the lower half of the cirque outline. The highest peak in the frequency distribution is highlighted by the yellow shade, representing the relatively flat part of the cirque threshold (actually cut by several streams for this cirque). (d) The extracted cirque threshold part (red line), with its middle point (green dot) as the cirque threshold focus. The yellow contour-line band (290 – 300 m) corresponds to the elevation range of the yellow shade in (c).

The cirque threshold foci derived using the second approach are more consistent with the geomorphological definition of the cirque focus, avoiding asymmetric position of the stream on the threshold, which could be related to post-glacial erosion. However, use of the modal elevation bin of the histogram in determining the cirque threshold may have issues for some unusual cirque topographies. For example, some cirques may contain relatively flat ridgelines on the low halves of the outlines, resulting in multiple histogram peaks and the highest frequency one may not correspond to the cirque threshold.

2.3 Cirque metrics and calculation methods

For each cirque, ACME2 outputs 49 morphometrics and 3 metadata attributes related to input datasets. The former are grouped into cirque location, size, shape, slope, aspect, altitude, axis-related, and catchment-related metrics (Table 1).

Three metadata attributes, *Projection*, *DEMresolution*, and *FocusMethod*, are related to the input datasets and the method to derive the threshold foci. These could be particularly useful to compare cirque metrics extracted from different DEM resolutions, map projections, and threshold methods. *Projection* is the map projection of the input cirque outlines and the DEM, including UTM zone if applicable. *DEMresolution* is the spatial resolution of the DEM. *FocusMethod* is to record which of three methods (mainstream exit, threshold midpoint, or user-specified) was used to derive the threshold foci.

ACME2 derives the attributes related to the centroid location of each cirque outline for dataset comparison, mapping and regional trend analyses. These location-related attributes include both geographic and grid coordinates: longitude (*Lon*), latitude (*Lat*), easting (*Easting*), and northing (*Northing*).

Seven metrics are related to cirque size: length (*L*), width (*W*), height (*H*), cirque size (*CS*), perimeter (*Perimeter*), planar area (*A2D*), and three-dimensional (3D) surface area (*A3D*). *L* and *W* are the same metrics as in the original ACME, measuring along the length and width axes that are determined using the same approach as ACME based on the cirque outline and threshold focus. *H* is the height range of the cirque, corresponding to *Z_range* (*Z_max – Z_min*) in ACME. *CS* is defined as the cubic root of *L**W*H* (Evans, 2006; Barr and Spagnolo, 2013, 2014, 2015; Delmas et al., 2015; Li et al., 2023):

$$CS = \sqrt[3]{L * W * H} \quad (1)$$

Cirque size (*CS)* provides a useful overall measure of size in the same units as *L*, *W* and *H*. *L**W*H* is not used as a measure of cirque volume as it is not possible to estimate the volume eroded to form a cirque unless the preglacial land surface is known. *Perimeter* is the length of the outline as in ACME, and *A2D* and *A3D* (see below) correspond to *Area_2D* and *Area_3D* in the original ACME.

Seven metrics are related to cirque shape. The length/width ratio (*L_W*) and circularity (*Circular*), are the same as ACME. ACME2 adds the length/height ratio (*L_H*), width/height ratio (*W_H*), and surface area/planar area ratio (*A3D_A2D*). Plan closure (*Plan_clos*) was in ACME but there are different methods for its calculation. Fig. 3a illustrates the plan closure calculation method in ACME, which is determined as 360° minus the acute angle between the cirque “midpoint” (or “centroid”) and start and end points along the mid-alt (altitude) contour (Spagnolo et al., 2017). The “midpoint” is determined as the intersection point of the two lines that bisect lines from the center of the mid-altitude contour to each end of that contour, corresponding to the center point of the circle defined by the start, end, and center points of the mid-alt contour (Fig. 3a).

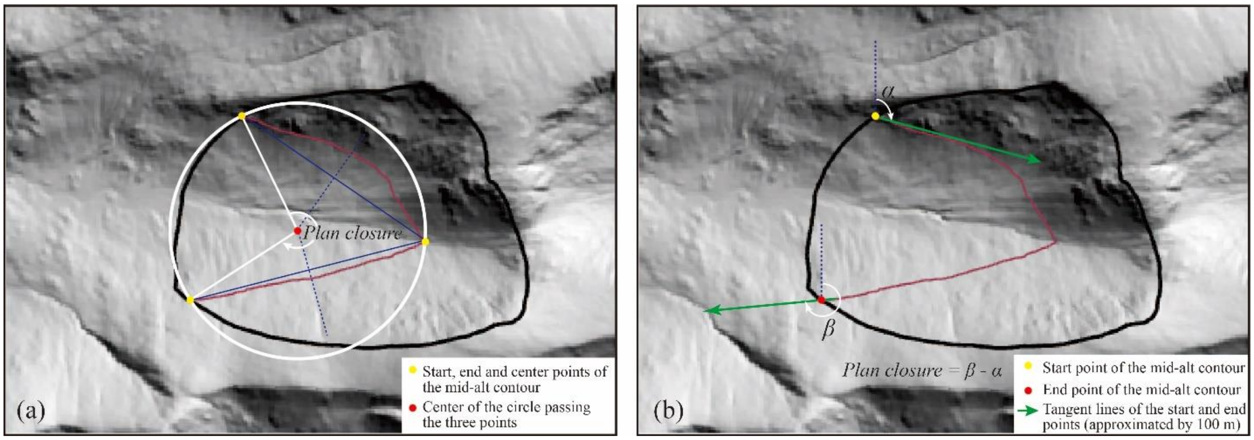

Fig. 3 The method to calculate plan closure in ACME (a), which is different from the manual method (b) of Evans and Cox (1995). The black polygon is the cirque outline, and the red line is the mid-altitude contour.

The above method for determining plan closure is different from the manual approach of Evans and Cox (1995), which derives the plan closure based on the azimuthal difference between the end tangent line direction (approximated by 100 m of contour) and the start tangent line direction (approximated by 100 m) along the mid-altitude contour (Fig. 3b). This manual method is easier to implement in the map measurement of cirque plan closure. In ACME2 another plan closure metric (*Plan_closISE*) is added based on the implementation of this manual method and the plan closure from the original ACME is renamed to *Plan_closSPA*.

In terms of slope-related metrics, in addition to the mean slope (*Slope_mean*) as in ACME, ACME2 adds the maximum (*Slope_max*) and minimum (*Slope_min*) slopes within the cirque, and profile closure (*Prof_clos*), which were used by Evans and Cox (1995). *Prof_clos* is defined as the difference between the maximum and minimum slopes within the cirque. Because a cirque usually requires both a floor and a headwall, three slope related metrics are also added: the percent of cirque area with slopes > 33°, representing the headwall (*Slpgt33*); the percent of cirque area with slopes < 20°, representing the floor (*Slplt20*), and the percent of cirque area with slopes between 20° and 33° (*Slp22to33*). Large values of the latter suggest indistinct development of cirque form, i.e. limited concavity.

ACME2 includes three metrics for aspect of the whole cirque. *Aspectmean* is the same as in ACME, derived as the vector mean of the aspect values of all cells within a cirque. Because aspect-related regressions are based on Fourier regressions with the cosine and sine components of aspect, ACME2 saves these two components as two metrics: *Asp_east* (the sine component) and *Asp_north* (the cosine component).

Seven metrics are related to cirque altitudes. The minimum, maximum, and mean altitudes of the cirque (*Z_min*, *Z_max*, and *Z_mean*, respectively) are the same as from ACME. In addition, the median (*Z_median*) and middle (*Z_mid*) altitudes are added in ACME2.

$$Z\_mid = \frac{Z\_\max + Z\_min}{2} \quad (2)$$

The hypsometric maximum (*Hypsomax*) and integral (*HI*) are also included but based on different calculation methods from ACME. ACME slices cirque topography into a set of elevation bins and uses the elevation distribution over these bins to derive the hypsometric maximum and integral values. The calculation process is usually time consuming, and the values are sensitive to the specification of bin width. As discussed in Pike and Wilson (1971), the *HI* value is mathematically the same as the elevation-relief ratio that is defined as:

$$HI = E\_ratio = \frac{Z\_\text{mean} - Z\_min}{Z\_\text{max} - Z\_min} \qquad (3)$$

where *Z_min*, *Z_max*, and *Z_mean* values are easily derived in the DEM; therefore, it is much quicker to derive *HI* in this manner and the derived value is also not affected by bin width. Similarly, in ACME2 *Hypsomax* is determined as the highest mode of the cirque elevations. A comparison of the *HI* values of 155 cirques in the English Lake District (Clark et al., 2018), indicates that the values derived using the ACME approach based on a 20-m bin width (elevation interval) and those based on the elevation-relief ratio approach in ACME2 are highly correlated ($r > 0.97$), with small differences probably caused by using the 20-m elevation interval (Fig. 4a). A similar comparison also indicates a high correlation between the *Hypsomax* values derived by ACME2 and ACME (Fig. 4b).

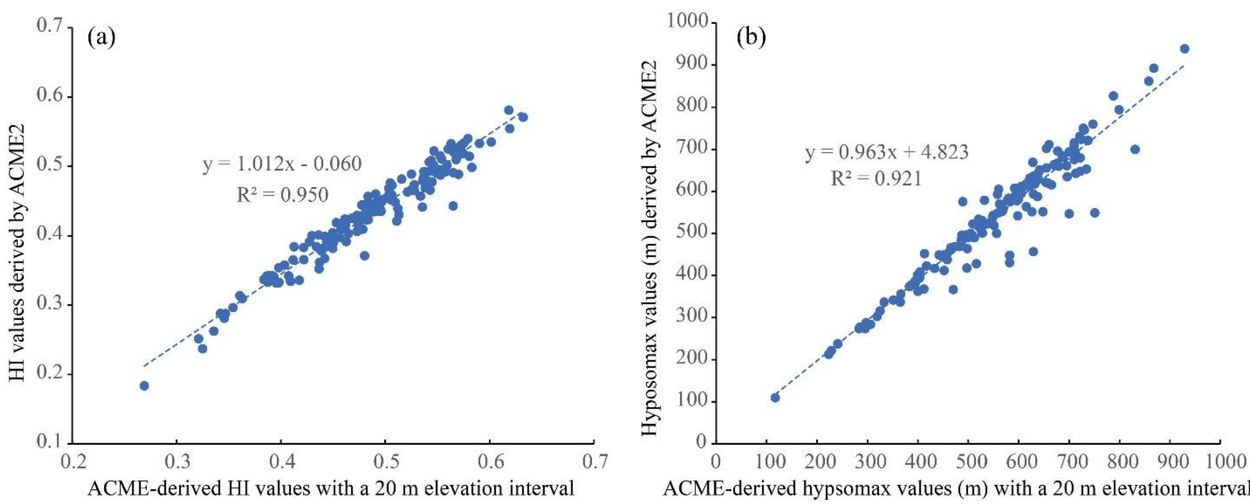

Fig. 4 The comparison of *HI* (a) and *Hypsomax* (b) values derived using ACME with a 20-m elevation interval and by ACME2, based on 155 cirques from the English Lake District (Clark et al., 2018).

Table 1. The list of cirque metrics and related attributes in ACME2.

Group	ACME2 metrics	Corresponding ACME metrics	Definition
Dataset (3)	*Projection*		The map projection of the input cirque outlines. Must be a projected coordinated system, with type and zone (UTM only).
	DEMresolution		The spatial resolution of the DEM. Must be in meters to ensure the correct calculations
	FocusMethod		The method to derive the threshold points: mainstream exit, threshold midpoint, and user specified
Location (4)	*Lon*		The longitude of the cirque centroid point [decimal degrees]
	Lat		The latitude of the cirque centroid point [decimal degrees]
	Easting		The easting (x coordinate) of the cirque centroid point [km]
	Northing		The northing (y coordinate) of the cirque centroid point [km]
Size (7)	*L*	*L*	Length of median axis [m]
	W	*W*	Width: Maximum, at right angles to axis, through cirque centroid [m]
	H	*Z_range*	height: the *Z_max* – *Z_min* [m]
	CS		Cirque size: the cubic root of *L*W*H* [m]
	Perimeter	*Perimeter*	The perimeter of the cirque outline [m]
	A2D	*Area_2D*	The cirque 2D (map) area [m^2]
	A3D	*area_3D*	The cirque 3D (surface) area [m^2]
Shape (7)	*L_W*	*L_W*	Length/Width ratio
	L_H		Length/Height ratio
	W_H		Width/Height ratio
	A3D_A2D		The 3D area / 2D area ratio for the cirque
	Circular	*Circular*	The circularity index
	Plan_closSPA	*Plan_clos*	The plan closure derived using the original ACME method [degrees]
	Plan_closISE		The plan closure derived using the method that is consistent with Evans' manual method [degrees]
Slope (7)	*Slope_mean*	*Slope_mean*	The mean slope of the cirque [degrees]
	Slope_max		The maximum slope of the cirque [degrees]
	Slope_min		The minimum slope of the cirque [degrees]

	Prof_clos		The difference between the maximum and minimum slope within the cirque [degrees]
	Slpgt33		The percentage of the cirque area with steep slopes of >33°
	Slplt20		The percentage of the cirque area with gentle slopes of <20°
	Slp20to33		The percentage of the cirque area with slopes between 20° and 33°
Aspect (3)	*Aspectmean*	*Aspectmean*	The vector mean aspect of all points within the cirque. *Note that this metric is a circular variable and cannot be summarized using the regular linear method* [degrees]
	Asp_east		The sine value of the *Aspectmean*
	Asp_north		The cosine value of the *Aspectmean*
Altitude (7)	*Z_min*	*Z_min*	The minimum elevation of the cirque [m]
	Z_max	*Z_max*	The maximum elevation of the cirque [m]
	Z_mean	*Z_mean*	The mean elevation of the cirque [m]
	Z_median		The median elevation of the cirque [m]
	Z_mid		The middle elevation of the cirque: (*Z_max* + *Z_min*) / 2 [m]
	Hypsomax	*hypsomax*	The highest mode of the cirque elevations. Revised: no contour interval is needed to derive this metric [m]
	HI	*HI*	Hypsometric integral. Revised as Elevation-relief ratio. No contour interval is needed for the calculation
Axis* (12)	*Axprofclos*		Profile closure axial (the maximum and minimum slope difference along the length axis) [degrees]
	Axhli		The height-length integral along the length axis
	Axasp		The aspect of the median axis, facing outward. *Note that this metric is a circular variable and cannot be summarized using the regular linear method* [degrees]
	Axgrad		The overall gradient along the median axis, arctan (*Axamp/L*) [degrees]
	Axamp		The amplitude (elevation difference) along the median axis [m]
	L_Exp_A		The best-fit "a" value of the longitudinal profile along the median axis using the exponential model $y = a*e^{bx}$.
	L_Exp_B		Axial concavity: the longitudinal profile's best-fit "b" value along the median axis using the exponential model $y = a*e^{bx}$.
	L_Exp_R2		Exponential fit: the best-fit R^2 value of the longitudinal profile along the median axis using the exponential model $y = a*e^{bx}$
	L_Kcurv_C		The best-fit "c" value of the model $y = (1-x)*e^{cx}$

	L_Kcurv_R2	k-curve fit: The best-fit R^2 value of the model $y = (1-x)*e^{cx}$
	W_Quad_C	Quadratic concavity: the best-fit "c" value of the model $y = a + bx + cx^2$
	W_Quad_R2	Quadratic fit: the best-fit R^2 value of the model $y = a + bx + cx^2$
Catchment (2)	*Maxabalt*	The maximum altitude draining into the cirque [m]
	Pctabarea	The percentage of a cirque area cut into the catchment area above the cirque threshold

*All curve-fitting coefficients for the axis-related metrics are based on meters.

In addition to the above metrics related to the whole cirque, ACME2 also derives 12 metrics related to the median axis that defines cirque length. *Axprofclos* is the profile closure (maximum slope - minimum slope) along this length (median) axis. *Axhli* is the height-length integral along the axis, in two dimensions rather than the three of the *HI* for the whole cirque. *Axasp*, *Axamp,* and *Axgrad* are respectively the aspect (facing outward), amplitude (elevation difference), and overall gradient (arctan (*Axamp*/*L*), in degrees) along the length (median) axis. *Axasp* is the same as the 'axis aspect' of Evans and Cox (1995). Two types of curve-fitting are also conducted for the topographic profile along the length (median) axis. One is to fit the profile using an exponential function:

$$y = a\,e^{bx} \tag{4}$$

where y is the height above the threshold midpoint, x is the horizontal distance away from the threshold focus along the median axis, and a and b are coefficients. The coefficient, b, is a measure of axial concavity. Three metrics, *L_Exp_A*, *L_Exp_B*, and *L_Exp_R2*, are used to save the coefficients a, b and the R^2 value of the curve fitting, respectively. In addition to the exponential function, Krause et al. (2022) proposed a K-curve function to describe the concavity of cirque longitudinal profile based on the following equation:

$$y = (1 - x)\, e^{cx} \quad (5)$$

where *y* and *x* are the normalized values from 0 to 1 for the height of the profile and horizontal distance away from the highest point, respectively. The coefficient, *c*, is a measure of the shape of the longitudinal profile. The more negative the value of *c*, the greater the concavity of the longitudinal profile. This coefficient has been used to discriminate between cirques and non-cirque valley heads (Krause et al., 2022; Jia et al., 2023). Note that the profiles in Krause et al. (2022) differ from ACME2's, as the former do not follow the median axis and generally stop short of the threshold (see their Fig. 3). In ACME2, two metrics, *L_Kcurv_C* and *L_Kcurv_R2,* are introduced to extract the coefficient *c* and the R^2 value for this function fitted to the ACME2 median axis.

A topographic profile along the width axis represents the cross-sectional profile of the glacial valley within the cirque part. The cross-sectional profile of a glacial valley can be described using a power function (Svensson, 1959; Graf, 1970; Wheeler, 1984; Harbor, 1990; James, 1996; Li et al., 2001) or a quadratic function (James, 1996; Li et al., 2001). Due to the uncertainty of the power function caused by the selection of the original point to divide the cross-section into two halves, we only applied the quadratic function to fit the cross-sectional profile:

$$y = a + bx + cx^2 \quad (6)$$

where *y* and *x* are the height and horizontal distance from the start point of the cross-section, respectively, and *a*, *b*, and *c* are coefficients. Both *a* and *b* are relative to the selection of the original point, while c describes the concavity and relative wideness of the valley bottom (quadratic concavity). Two metrics, *W_Quad_C* and *W_Quad_R2*, are used to save the coefficient *c* and the R^2 value for the curve-fit of the quadratic function.

Cirques are located at glacial valley heads, but may not always reach the drainage divides, especially when cirques cut into a plateau. It is therefore important to measure how much the cirque glacier (or most likely glaciers, over multiple glaciations) eroded its upper catchment area and therefore potentially limited its elevation, as hypothesised by the glacial buzzsaw (Brozović et al., 1997; Mitchell and Montgomery, 2006; Egholm et al., 2009). ACME2 introduces two metrics, *Maxabalt* and *Pctabarea*, to describe the extent of cirque cutting into the valley head catchment or plateau (Fig. 5). *Maxabalt* records the maximum altitude draining into the cirque and *Pctabarea* represents the percentage of a cirque area cut into the catchment area above the cirque threshold. A glacial buzzsaw effect is supported in an area where the cirque *Z_max* values are similar to *Maxabalt* and the cirque *Pctabarea* values are close to 100%.

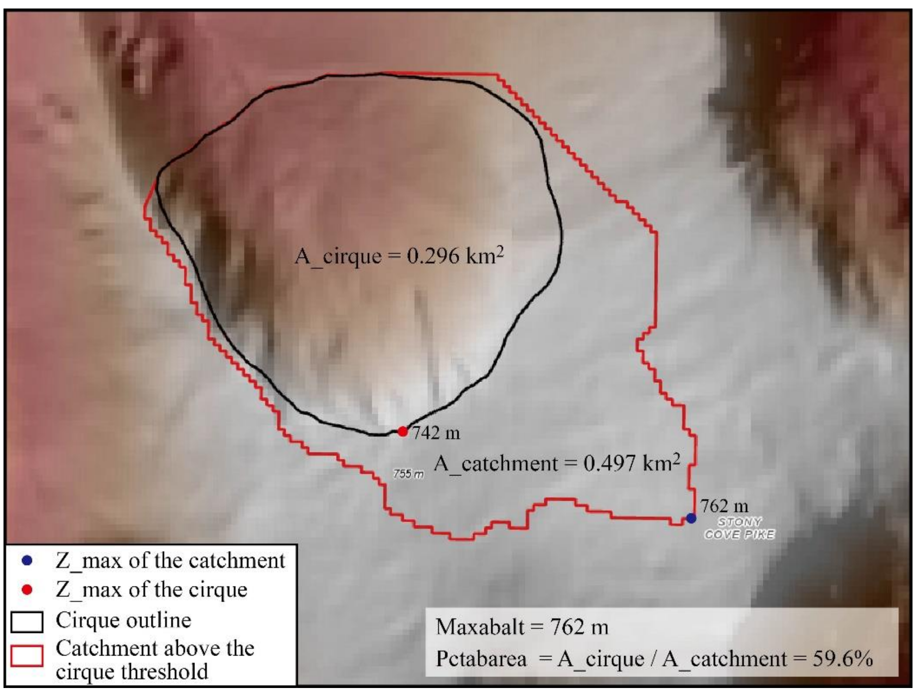

Fig. 5 An example cirque from the English Lake District, to illustrate the definitions of *Maxabalt* and *Pctabarea* related to the catchment above the cirque threshold.

The result of these changes is that, in addition to providing a series of new variables, ACME2 measures or approximates 12 of the 19 measured circular or ratio scale variables and 5 of the 6 calculated variables in Evans and Cox (1995). ACME2 does not provide the four ordinal and nominal variables, two contextual (relief) variables, the number of cols, the three variables related to the floor, and the two related to the headwall. Careful distinction of cirque floor and headwall requires considerable further interpretation and digitizing (as in Mîndrescu and Evans, 2014). ACME2 approximates the distinction by calculating percentages of slopes above 33° and below 20°, providing their relative sizes. The three variables (grade, lake?, and type) defined in Evans and Cox (1995) require subjective judgment or additional work and input data (e.g. satellite imagery, geological maps) that is beyond the scope of this effort.

3. Demonstration and comparison with the manually derived metrics

Digitized outlines are available for two areas with detailed measurements by manual methods from 1:20,000 and 1:5,000 contour maps, respectively. This permits a comparison between ACME2 and manual analyses, using correlation coefficients for those variables with comparable definitions (i.e. those aiming to measure the same attribute).

The first dataset comprises 51 cirques in the northern Shulaps Range, British Columbia Coast Mountains. The cirque outlines were digitized on Google Earth by I.S. Evans and metrics were measured from topographic contour maps (1:20,000 with 20 contour interval). Three 1-arc-second DEMs are used to derive cirque metrics. All DEMs are download from OpenTopography (https://portal.opentopography.org/). The first is the 1 arc-second DEM from United States Geological Survey (USGS, 2021). This dataset is derived from various data sources, such as high-resolution air photos and airborne LiDAR, with trees and buildings removed (it has complete coverage of the conterminous U.S.A., plus much of Canada and Mexico, and partial coverage of Alaska). The second is the Shuttle Radar Topography Mission (SRTM) 1 arc-second global elevation data (NASA, 2013) from a mission conducted during February 11-22, 2000: https://www.usgs.gov/centers/eros/science/usgs-eros-archive-digital-elevation-shuttle-radar-topography-mission-srtm-1-arc?qt-science_center_objects=0#qt-science_center_objects (NASA, 2013). The third DEM is the 1 arc-second Copernicus (COP) Global DEM, which is derived from an edited WorldDEM produced based on the radar satellite data acquired during the TanDEM-X Mission by the German Aerospace Centre (DLR) and Airbus Defence and Space (ESA, 2021). At 51° North, 1 arc-second is 19.5 x 30.9 m. All DEMs are projected to the UTM projection (Zone 10N) with 25 m resolution (at this latitude) for the calculation of cirque metrics.

Results from the ACME2 calculation and the manual method (Table 2) are very close (almost identical) for size variables and altitude variables. Although the manual method used median axis midpoint and ACME2 uses the centroid of area, the results for Easting and Northing are almost identical. The last five variables give good-moderate correlations reflecting differences between each DEM and the contour information. Profile closure is the difference between maximum and minimum gradients, which are measured differently in the two approaches. For the DEMs, slope gradients are calculated from a quadratic for a 3 x 3 (i.e. 75 x 75 m) window, whereas following Evans and Cox (1995) maximum gradient is measured over 30 m or more vertically (i.e. at least two 20 m contours in Shulaps) and minimum gradient from greatest contour spacing, here for 20 m contours. Thus, profile closures and axial gradients will be comparable only where gradient extremes are measured at similar resolution, from similar DEMs or contour maps.

Comparing the three DEMs, SRTM DEM generally gives the lowest correlations with manual results, especially for maximum slope, profile closure and axial gradient. It is somewhat better than COP DEM only for plan closure, where both are worse than USGS DEM. Because of radar shadows, SRTM DEM and COP DEM have low precision where gradients exceed 40°, as on headwalls. The COP DEM shows considerable improvement over SRTM DEM, and thus gives much higher correlations for maximum slope and profile closure. The USGS DEM generally has higher correlations than COP DEM, except for minimum slope and length (Table 2).

Table 2. Correlations, for 51 cirques in northern Shulaps, between ACME2 results and those manually measured by Evans from contour maps (1:20,000 with 20 contour interval) and Google Earth. Comparisons are made for both methods, for three 25 m DEMs: USGS, COP and SRTM.

Variable	*USGS mainstream*	*COP mainstream*	*SRTM mainstream*	*USGS midpoint*	*COP midpoint*	*SRTM midpoint*
Easting	0.9994	0.9994	0.9994	0.9994	0.9994	0.9994
Northing	0.9998	0.9998	0.9998	0.9998	0.9998	0.9998
perimeter	0.9997	0.9997	0.9997	0.9997	0.9997	0.9997
z_min	0.9997	0.9997	0.9996	0.9997	0.9997	0.9996
z_max	0.9990	0.9991	0.9980	0.9990	0.9991	0.9980
z_range	0.9982	0.9982	0.9982	0.9982	0.9982	0.9982
length	0.9850	0.9901	0.9910	0.9922	0.9931	0.9907
width	0.9790	0.9893	0.9883	0.9867	0.9861	0.9812
max altitude above	0.9776	0.9338	0.9277	0.9776	0.9338	0.9277
axial gradient	0.8453	0.8355	0.7192	0.8708	0.8525	0.8359
plan closure	0.8134	0.7883	0.8059	0.8134	0.7883	0.8059
profile closure	0.8401	0.8033	0.6558	0.8398	0.8033	0.6558

max. slope	0.8734	0.7988	0.6161	0.8734	0.7988	0.6161
min. slope	0.6987	0.7364	0.7309	0.6987	0.7364	0.7309
axial aspect (circular *r*)*	0.8690	0.8670	0.8260	0.8690	0.9090	0.8880

* circular correlation for aspect takes account of the 0° = 360° problem.

Overall, the correlations for cirque altitude and size variables of over 0.92 from SRTM, 0.93 from COP, and 0.97 from USGS DEMs give us confidence in comparing ACME2 results with published results using manual methods. More caution is needed when comparing the variables for slope and closure. Slope estimates are inevitably sensitive to DEM resolution and quality, as they are to contour interval and quality: comparisons are fully valid only when the same source and method are used. Profile closure is the difference between two slopes. Even so, correlations exceed 0.81 for USGS DEM and 0.78 for COP DEM, except for minimum slope. For plan closure it has proved difficult to produce results close to manual methods (Fig. 6): it is accepted that the automated method can produce good results (*r* from 0.78 to 0.81 for *Plan_closISE*) and for a much greater number of cirques than the Evans and Cox (1995) manual method which it supersedes. The correlation between the plan closure derived by the original ACME (*Plan_closSPA* in ACME2) and the manually derived values was much lower (*r* from 0.45 to 0.49) due to their different definitions, as illustrated in Fig. 3.

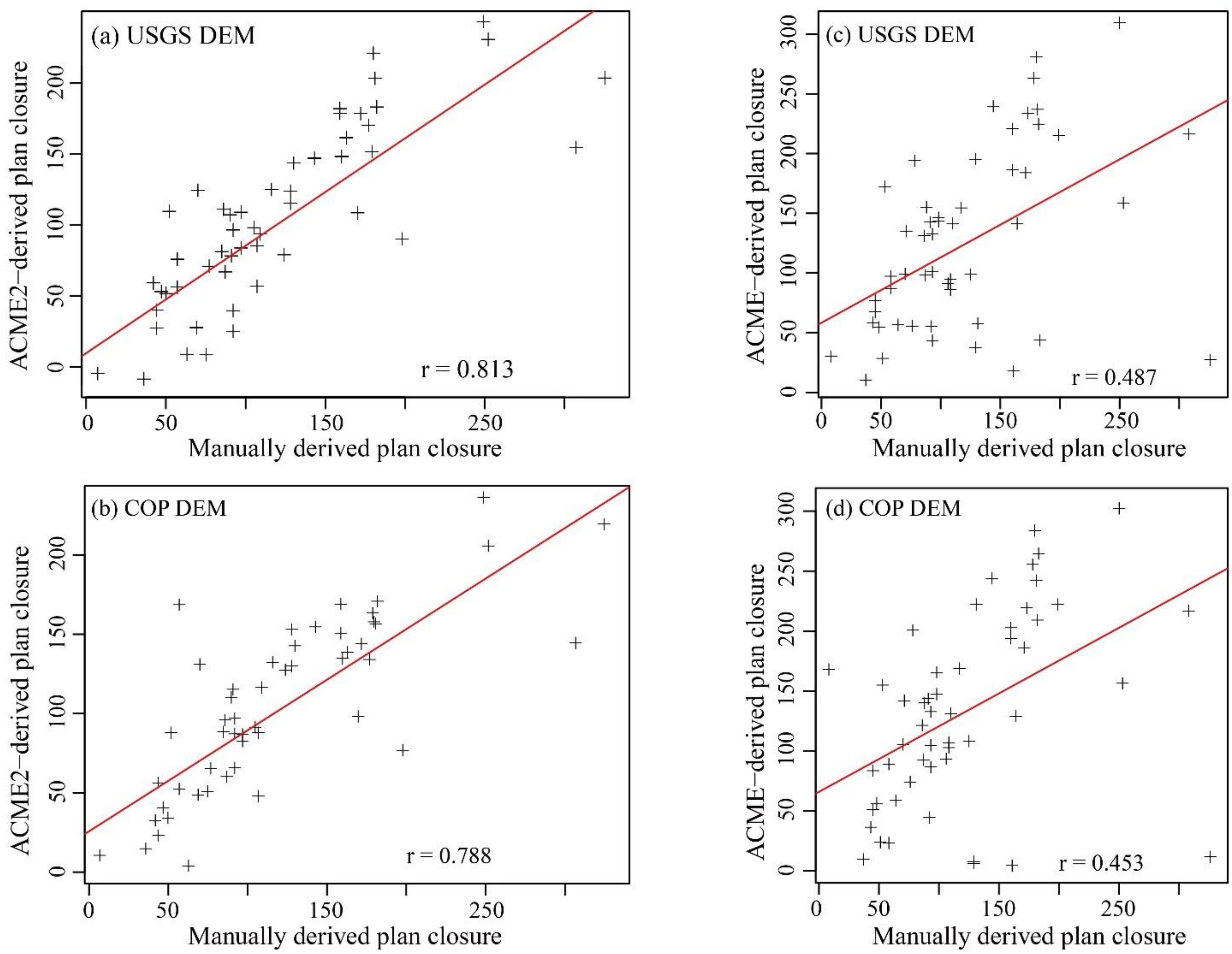

Fig. 6 Correlations between ACME2-derived plan closure (*Plan_closISE*) and Evans' manual derived values for the 51 cirques in northern Shulaps, British Columbia, for USGS (a), and COP DEMs (b). Similar correlations for the plan closure values derived using ACME (*Plan_closSPA*; c, d).

A more complex comparison can be made from the second dataset of outlines, for 155 cirques in the English Lake District. Cirque outlines were digitized in the Britice project (Clark et al., 2018) for cirques identified by Evans and Cox (1995) and Evans (2015), but independently, without reference to Evans' outlines. Thus, the differences considered here combine differences due to subjective differences in outline delimitation with differences due to technique and are expected to be greater (i.e. produce lower correlations). The Evans outlines were drawn on 1:5,000 enlargements of Ordnance Survey 1:10,000 scale photogrammetric maps with 10 m contour intervals, and validated using air photos (black and white) and field observations. The Britice outlines were digitized using Bing Maps imagery, Google Earth, and the NEXTMap (5 m) DEM.

The DEM used for the calculation of cirque metrics is the LiDAR Composite 10-m DTM (Digital Terrain Model), which is resampled from the LiDAR Composite 2022 2-m DTM using a bilinear resampling technique by the Environment Agency, United Kingdom, in 2022 (https://environment.data.gov.uk/dataset/ce8fe7e7-bed0-4889-8825-19b042e128d2). For comparison, the 1-arc second SRTM and COP DEMs are also used for the calculations. At this latitude, 54.5° N, 1 arc-second is 18.0 x 30.9 m. Both SRTM and COP DEMs are projected to the UTM projection (Zone 30N) and gridded at 24.7 m resolution.

The expectation of lower correlations, relative to those found in comparisons for the British Columbia cirques, due to the use here of different outlines does not occur for all of the calculated metrics (Table 3). Compared with Table 2, correlations are lower for z values. They are lower for plan closure and maximum altitude above, except with COP DEM. They are lower for maximum slope except with SRTM DEM. Correlations are higher for axial gradient, profile closure and aspect, and much higher for minimum slope. Manual measures of these variables may have been more accurate for the English Lake District maps with a 10 m contour interval than for Shulaps with a 20 m.

For both mainstream and midpoint methods for COP DEM, *r* exceeds 0.9 for altitudes, length, and z_range, approximates 0.9 for width, and exceeds 0.8 for minimum slope, axial gradient (except mainstream in SRTM DEM), and profile convexity (except SRTM DEM). The poorest correlations are for plan closure (0.79) and maximum slope (0.77). LiDAR DEM correlations are in similar order except that maximum slope improves to $r = 0.87$. SRTM DEM correlations are also similar except for the low correlation in axial gradient using the mainstream method ($r = 0.75$) and lower correlations for profile convexity ($r = 0.71$).

Table 3. Correlations, for 155 cirques in the English Lake District, between ACME2 results and those manually measured by Evans from enlarged contour maps (1:5,000 with 10 contour interval)

Variable	*Lidar10m mainstream*	*COP mainstream*	*SRTM mainstream*	*Lidar10m midpoint*	*COP midpoint*	*SRTM midpoint*
Easting	0.9999	0.9999	0.9999	0.9999	0.9999	0.9999
Northing	0.9997	0.9997	0.9997	0.9997	0.9997	0.9997
z_min	0.9792	0.9791	0.9802	0.9792	0.9791	0.9802
z_max	0.9877	0.9861	0.9876	0.9877	0.9861	0.9876
z_range	0.9374	0.9355	0.9404	0.9374	0.9355	0.9404
length	0.9332	0.9321	0.9323	0.9349	0.9382	0.9382
width	0.9029	0.8955	0.8840	0.8972	0.9020	0.9001
max altitude above	0.9669	0.9663	0.9151	0.9669	0.9663	0.9151
axial gradient	0.8433	0.8545	0.7492	0.8690	0.8764	0.8562
plan closure	0.7613	0.7939	0.7846	0.7613	0.7939	0.7846
profile closure	0.8643	0.8352	0.7057	0.8643	0.8352	0.7057
max. slope	0.8663	0.7735	0.6372	0.8663	0.7735	0.6372
min. slope	0.8534	0.8899	0.8447	0.8534	0.8899	0.8447
axis aspect (circular *r*)*	0.8840	0.8630	0.8290	0.9320	0.9300	0.9290

Note: Perimeter is not available for the Evans English Lake District data. * circular correlation for aspect takes account of the 0° = 360° problem.

4. Comparison of results from the two definitions of focus

Figs. 7 and 8 show the maps of the threshold points (foci) derived from the two methods for the 155 cirques in the English Lake District (Fig. 7) and the 51 cirques in the northern Shulaps Range, British Columbia, Canada (Fig. 8). Overall, the foci derived from the two methods match well in all three areas. It seems that the offsets between the two points for individual cirques are related to the DEM resolution. The median offset distance is about 3-4 cell sizes of the DEM, and the mean offset distance is about 4-5 cell sizes of the DEM. However, large differences of several hundred meters do exist for some cirques in each area. For those cirques, the users can manually check the two derived points and choose the suitable one or digitize a new threshold point for each cirque.

Choice of focus affects variables related to axis, length, and width, not those related to the perimeter or all pixels (e.g. slope), and not plan and profile closures or location. Differences between variables based on threshold midpoint foci and those based on mainstream exit foci are small (Tables 2 and 3).

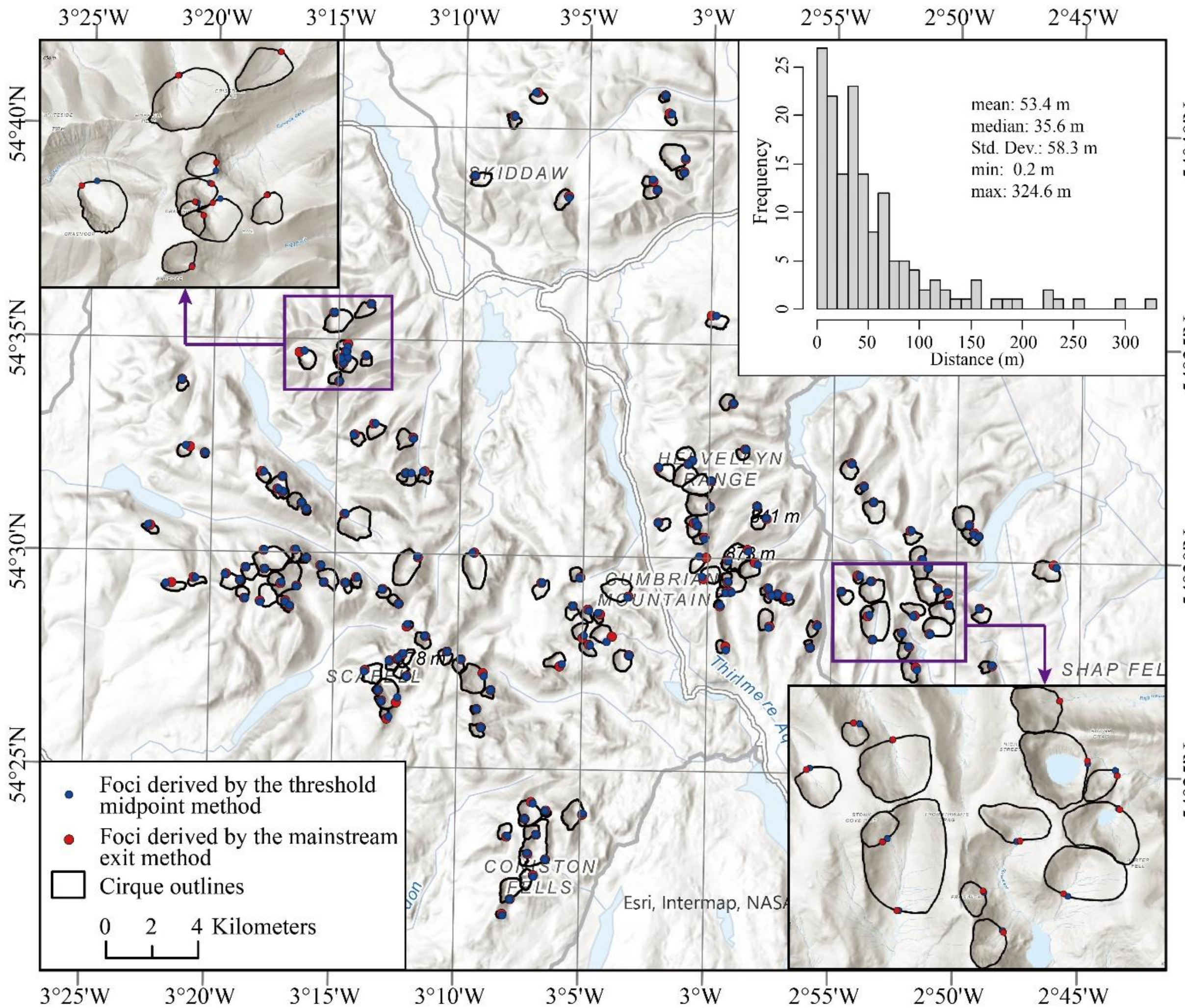

Fig. 7 Map of the cirque foci derived by the threshold midpoint and mainstream exit methods based on the 10-m LiDAR DEM for the 155 cirques in the English Lake District. The upper-right histogram shows the frequency distribution of the distance between the two points for each cirque. Two enlarged areas of the cirque focus points are illustrated on the upper-left and right-bottom maps.

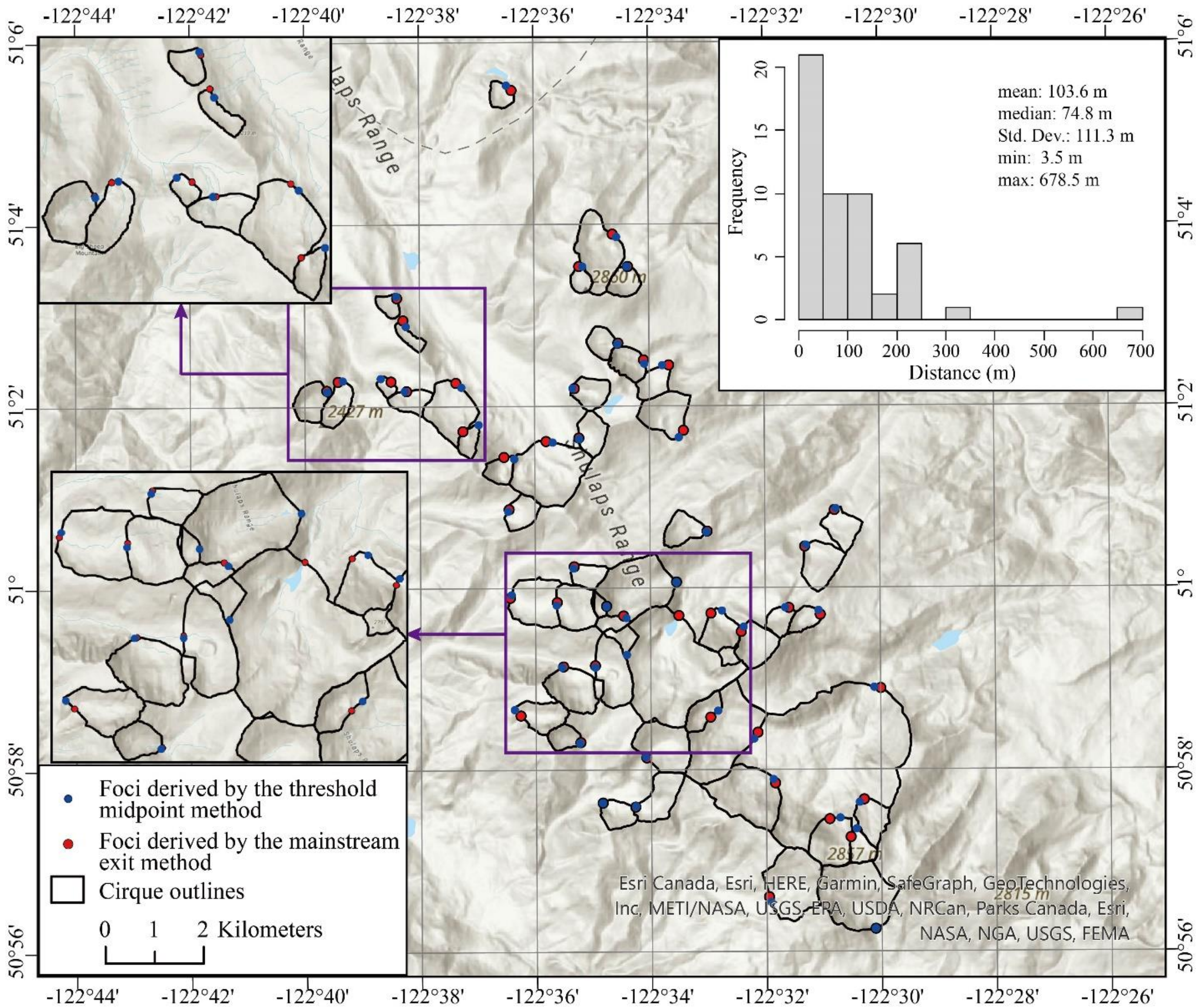

Fig. 8 Map of the cirque foci derived by the threshold midpoint and mainstream exit methods based on the COP DEM for the 65 cirques in the northern Shulaps Range, British Columbia Coast Mountains. The upper-right histogram shows the frequency distribution of the distance between the two points for each cirque. Two enlarged areas of the cirque focus points are illustrated on the upper-left and middle-left maps.

The midpoint method provides results much closer to the manual results than does the mainstream exit method (Table 2). For COP and USGS DEMs, it is also closer for length. For width, the mainstream exit is a little closer for COP and SRTM DEMs. From Table 3 (English Lake District), it is clear that for all three DEMs the ACME2 midpoint method come closer to the manual results than does the mainstream exit method, for length, axial gradient and especially for aspect. This is as expected, as Evans and Cox (1995) defined the focus as the threshold midpoint and used it as the starting point for the median axis. Note that neither method for foci, nor the manual estimation, necessarily takes the low point of the cirque, although they are expected to come close. For width (defined as orthogonal to the axis at half-way along the median axis in ACME but as maximum orthogonal to the axis in Evans and Cox (1995)), the results of COP and SRTM DEMs are closer to manual values when the midpoint method is used but the LiDAR DEM gives a somewhat higher *r* for mainstream.

Nevertheless, until more experience is gained with such results, definitions of foci should be checked carefully. In practice, we suggest deriving the threshold foci points using both the mainstream exit and threshold midpoint methods and comparing their differences. The midpoint method should provide comparability with previous manually measured variables, but the mainstream-exit method may be more reproducible.

5. Conclusions

In this paper, we introduce a revised and extended ArcGIS toolbox, ACME2, for cirque metric calculation. This extended toolbox includes two methods to automatically derive cirque foci and 49 morphometric and locational variables, as well as 3 input metadata attributes. ACME2 also improves the methods to derive the hypsometric integral and maximum; it adds a new method for plan closure to be more consistent with the original definition. The demonstration of this toolbox for 155 cirques in the English Lake District, and 51 cirques in the Shulaps Range, British Columbia, indicates high consistency with manual methods, with most high correlations characterized by $r > 0.90$. The differences result primarily from small differences in cirque outlines and from characteristics of the DEMs versus topographic maps used for the calculations.

Determination of the cirque focus, which is a required step to determine the median axis, is important as it has knock-on effects on axis-related variables including length and aspect. Two solutions presented here permit automation of the process. The 'mainstream exit' usually takes the lowest elevation point. The 'threshold midpoint' comes closer to the hitherto used method.

The validation of ACME2-derived metrics with manual techniques allows users to undertake meaningful comparisons with earlier studies. The addition of many new variables, e.g. for profiles and slope, permits a fuller description of cirque form and assessment of the degree of cirque development. Application to large datasets facilitates relation of these to controls of cirque erosion. Improved algorithms for some metrics increase the accuracy and computational efficiency. Flexibility is provided for the methods to determine cirque foci, including manual input. In conclusion, ACME2 allows for the rapid morphometric processing and thorough analysis of large datasets of cirques for palaeoclimate reconstruction and regional comparisons. Some of its tools and metrics could also be relevant to the morphological study of other landforms that can be precisely delineated (Evans, 2012).

Weblink

The ACME2 toolbox and its related python source codes are available on https://github.com/yingkui2003/ACME2. Users can download the zip file from this site, including the toolbox file and its associated python folder with the python code files, unzip it to their computer, and run these tools directly in ArcGIS 10.7, 10.8, ArcGIS Pro 2.8 or newer.

Acknowledgements:

This study was supported by the National Natural Science Foundation of China (No. 41971075). JCE acknowledges support from a NERC independent fellowship (NE/R014574/1). We thank the editor and two anonymous reviewers for their helpful comments and suggestions.

References

Anders, A.M., Mitchell, S.G., Tomkin, J.H., 2010. Cirques, peaks, and precipitation patterns in the Swiss Alps: Connections among climate, glacial erosion, and topography. Geology 38, 239–242. https://doi.org/10.1130/G30691.1.

Anders, N.S., Seijmonsbergen, A.C., Bouten, W., 2015. Rule set transferability for object-based feature extraction: an example for cirque mapping. Photogrammetric Engineering & Remote Sensing 81(6), 507-514. doi: https://doi.org/10.14358/PERS.81.6.507.

Andrews, J.T., Dugdale, R.E., 1971. Quaternary History of Northern Cumberland Peninsula, Baffin Island, N.W.T.: Part V: Factors Affecting Corrie Glacierization in Okoa Bay. Quaternary Research 1, 532–551. https://doi.org/10.1016/0033-5894(71)90063-9.

Barr, I.D., Ely, J.C., Spagnolo, M., Clark, C.D., Evans, I.S., Pellicer, X.M., Pellitero, R., Rea, B.R., 2017. Climate patterns during former periods of mountain glaciation in Britain and Ireland: Inferences from the cirque record. Palaeogeography, Palaeoclimatology, Palaeoecology 485, 466–475. https://doi.org/10.1016/j.palaeo.2017.07.001.

Barr, I.D., Ely, J.C., Spagnolo, M., Evans, I.S., Tomkins, M.D., 2019. The dynamics of mountain erosion: Cirque growth slows as landscapes age. Earth Surface Processes and Landforms

44, 2628–2637. https://doi.org/10.1002/esp.4688.

Barr, I.D., Spagnolo, M., 2013. Palaeoglacial and palaeoclimatic conditions in the NW Pacific, as revealed by a morphometric analysis of cirques upon the Kamchatka Peninsula. Geomorphology 192, 15–29. https://doi.org/10.1016/j.geomorph.2013.03.011.

Barr, I.D., Spagnolo, M., 2014. Testing the efficacy of the glacial buzzsaw: insights from the Sredinny Mountains, Kamchatka. Geomorphology 206, 230–238. https://doi.org/10.1016/j.geomorph.2013.09.026.

Barr, I.D., Spagnolo, M., 2015. Glacial cirques as palaeoenvironmental indicators: Their potential and limitations. Earth-Science Reviews 151, 48–78. https://doi.org/10.1016/j.earscirev.2015.10.004.

Barr, I.D., Spagnolo, M., Rea, B.R., Bingham, R.G., Oien, R.P., Adamson, K., Ely, J.C., Mullan, D.J, Pellitero, R., Tomkins, M.D., 2022. 60 million years of glaciation in the Transantarctic Mountains. Nature Communnications, 13, 5526. doi: 10.1038/s41467-022-33310-z.

Barr, I.D., Spagnolo, M., Tomkins, M.D., 2023. Glacial cirques in the Transantarctic Mountains reveal controls on glacier formation and landscape evolution. Geomorphology. https://doi.org/10.1016/j.geomorph.2023.108970.

Brozović, N., Burbank, D.W., Meigs, A.J., 1997. Climatic Limits on Landscape Development in the Northwestern Himalaya. Science 276, 571–574. https://doi.org/10.1126/science.276.5312.571.

Clark, C.D., Ely, J.C., Greenwood, S.L., Hughes, A.L.C., Meehan, R., Barr, I.D., Bateman, M.D., Bradwell, T., Doole, J., Evans, D.J.A., Jordan, C.J., Monteys, X., Pellicer, X.M., Sheehy, M., 2018. BRITICE Glacial Map, version 2: a map and GIS database of glacial landforms

of the last British–Irish Ice Sheet. Boreas 47, 11-e8. https://doi.org/10.1111/bor.12273.
Delmas, M., Gunnell, Y., Calvet, M., 2015. A critical appraisal of allometric growth among alpine cirques based on multivariate statistics and spatial analysis. Geomorphology 228, 637–652. https://doi.org/10.1016/j.geomorph.2014.10.021.
Egholm, D.L., Nielsen, S.B., Pedersen, V.K., Lesemann, J.-E., 2009. Glacial effects limiting mountain height. Nature 460, 884–887. https://doi.org/10.1038/nature08263.
Eisank, C., Drăguţ, L., Götz, J., Blaschke, T., 2010. Developing a semantic model of glacial landforms for object-based terrain classification—the example of glacial cirques. In: Addink, E.A., Van Coillie, F.M.B. (Eds.), GEOBIA-Geographic Object-Based Image Analysis. ISPRS Vol. No. XXXVIII-4/C7, pp. 1682–1777.
ESA (European Space Agency, Sinergise), 2021. Copernicus Global Digital Elevation Model. Distributed by OpenTopography. https://doi.org/10.5069/G9028PQB. Accessed: 2023-08-26.
Evans, I.S., 2012. Geomorphometry and landform mapping: what is a landform? Geomorphology, 137 (1), 94-106. In ‘Geospatial Technologies and Geomorphological Mapping’, Proceedings of the 41st Annual Binghamton Geomorphology Symposium. doi:10.1016/j.geomorph.2010.09.029.
Evans, I.S., 2015. The Lake District cirque inventory: updated. In McDougall D.A., Evans, D.J.A., The Quaternary of the Lake District: Field Guide, 65–82. Quaternary Research Association, London.
Evans, I.S., 2021. Glaciers, rock avalanches and the ‘buzzsaw’ in cirque development: Why mountain cirques are of mainly glacial origin. Earth Surface Processes and Landforms 46, 24–46. https://doi.org/10.1002/esp.4810.

Evans, I.S., 2006. Local aspect asymmetry of mountain glaciation: A global survey of consistency of favoured directions for glacier numbers and altitudes. Geomorphology 73, 166–184. https://doi.org/10.1016/j.geomorph.2005.07.009.

Evans, I.S., 1977. World-Wide Variations in the Direction and Concentration of Cirque and Glacier Aspects. Geografiska Annaler: Series A, Physical Geography 59, 151–175. https://doi.org/10.1080/04353676.1977.11879949.

Evans, I.S., Cox, N.J., 2017. Comparability of cirque size and shape measures between regions and between researchers. Zeitschrift für Geomorphologie. Supplementary issues. 61, 81–103. https://doi.org/10.1127/zfg_suppl/2016/0329.

Evans, I.S., Cox, N.J., 1995. The form of glacial cirques in the English Lake District, Cumbria. Zeitschrift für Geomorphologie 175–202. https://doi.org/10.1127/zfg/39/1995/175.

Federici, P.R., Spagnolo, M., 2004. Morphometric analysis on the size, shape, and areal distribution of glacial cirques in the Maritime Alps (Western French-Italian Alps). Geografiska Annaler Series A Physical Geography 86 (3), 235–248.

Gardner, J.S., 1987. Evidence for Headwall Weathering Zones, Boundary Glacier, Canadian Rocky Mountains. Journal of Glaciology 33, 60–67. https://doi.org/10.3189/S0022143000005359.

Graf, W.L., 1970. The Geomorphology of the Glacial Valley Cross Section. Arctic and Alpine Research 2, 303–312. https://doi.org/10.1080/00040851.1970.12003589.

Harbor, J.M., 1990. A discussion of hirano and Aniya’s (1988, 1989) explanation of glacial-valley cross profile development. Earth Surface Processes and Landforms 15, 369–377. https://doi.org/10.1002/esp.3290150408.

James, L.A., 1996. Polynomial and Power Functions for Glacial Valley Cross-Section

Morphology. Earth Surface Processes and Landforms 21, 413–432. https://doi.org/10.1002/(SICI)1096-9837(199605)21:5<413::AID-ESP570>3.0.CO;2-S.

Jia, T., Qin, C.-Z., Fu, P., Brusic, V., 2023. Applicability of longitudinal profiles for glacial cirque classification. https://doi.org/10.5281/zenodo.7834856.

Krause, D., Fišer, J., Křížek, M., 2022. Morphological differences of longitudinal profiles between glacial cirques and non-glacial valley heads, described by mathematical fitting. Geomorphology 404, 108183. https://doi.org/10.1016/j.geomorph.2022.108183.

Li, S., Zhang, Q., Wang, J., 2022. Cirques of the Southeastern Tibetan Plateau and Their Links to Climatic and Non-Climatic Factors. International Journal of Environmental Research and Public Health 19, 13104. https://doi.org/10.3390/ijerph192013104.

Li, Y., Liu, G., Cui, Z., 2001. Glacial valley cross-profile morphology, Tian Shan Mountains, China. Geomorphology 38, 153–166.

Li, Y., Zhao, Z., 2022. AutoCirque: An automated method to delineate glacial cirque outlines from digital elevation models. Geomorphology 398, 108059. https://doi.org/10.1016/j.geomorph.2021.108059.

Li, Y., Zhao, Z., Evans, I.S., 2023. Cirque morphology and palaeo-climate indications along a south-north transect in High Mountain Asia. Geomorphology 431, 108688. https://doi.org/10.1016/j.geomorph.2023.108688.

Mîndrescu, M., Evans, I.S., 2014. Cirque form and development in Romania: Allometry and the buzzsaw hypothesis. Geomorphology 208, 117–136. https://doi.org/10.1016/j.geomorph.2013.11.019.

Mîndrescu, M., Evans, I.S., Cox, N.J., 2010. Climatic implications of cirque distribution in the Romanian Carpathians: palaeowind directions during glacial periods. J. Quat. Sci. 25,

875–888. https://doi.org/10.1002/jqs.1363.
Mitchell, S.G., Humphries, E.E., 2015. Glacial cirques and the relationship between equilibrium line altitudes and mountain range height. Geology 43, 35–38. https://doi.org/10.1130/G36180.1.
Mitchell, S.G., Montgomery, D.R., 2006. Influence of a glacial buzzsaw on the height and morphology of the Cascade Range in central Washington State, USA. Quaternary Research 65, 96–107. https://doi.org/10.1016/j.yqres.2005.08.018.
NASA, 2013. Shuttle Radar Topography Mission (SRTM) Global. Distributed by OpenTopography. https://doi.org/10.5069/G9445JDF. Accessed: 2023-08-26.
Nelson, F.E.N., Jackson, L.E., 2002. Cirque forms and alpine glaciation during the Pleistocene, west-central Yukon 16.
Oien, R.P., Barr, I.D., Spagnolo, M., Bingham, R.G., Rea, B.R., Jansen, J., 2022. Controls on the altitude of Scandinavian cirques: What do they tell us about palaeoclimate? Palaeogeography, Palaeoclimatology, Palaeoecology 600, 111062. https://doi.org/10.1016/j.palaeo.2022.111062.
Oien, R.P., Spagnolo, M., Rea, B.R., Barr, I.D., Bingham, R.G., 2020. Climatic controls on the equilibrium-line altitudes of Scandinavian cirque glaciers. Geomorphology 352, 106986. https://doi.org/10.1016/j.geomorph.2019.106986.
Pedraza, J., Carrasco, R.M., Villa, J., Soteres, R.L., Karampaglidis, T., Fernández-Lozano, J., 2019. Cirques in the Sierra de Guadarrama and Somosierra Mountains (Iberian Central System): Shape, size and controlling factors. Geomorphology 341, 153–168. https://doi.org/10.1016/j.geomorph.2019.05.024.
Pike, R.J., Wilson, S.E., 1971. Elevation-Relief Ratio, Hypsometric Integral, and Geomorphic

Area-Altitude Analysis. GSA Bulletin 82, 1079–1084. https://doi.org/10.1130/0016-7606(1971)82[1079:ERHIAG]2.0.CO;2.

Principato, S.M., Lee, J.F., 2014. GIS analysis of cirques on Vestfirðir, northwest Iceland: implications for palaeoclimate. Boreas 43, 807–817. https://doi.org/10.1111/bor.12075.

Sanders, J.W., Cuffey, K.M., Moore, J.R., MacGregor, K.R., Kavanaugh, J.L., 2012. Periglacial weathering and headwall erosion in cirque glacier bergschrunds. Geology 40, 779–782. https://doi.org/10.1130/G33330.1.

Scuderi, L.A., Nagle-McNaughton, T., 2022. Automated neural network identification of cirques. Physical Geography 43, 24-51. doi: 10.1080/02723646.2021.1928871.

Seif, A., Ebrahimi, B., 2014. Combined use of GIS and experimental functions for the morphometric study of glacial cirques, Zardkuh Mountain, Iran. Quaternary International 353, 236–249.

Spagnolo, M., Pellitero, R., Barr, I.D., Ely, J.C., Pellicer, X.M., Rea, B.R., 2017. ACME, a GIS tool for Automated Cirque Metric Extraction. Geomorphology 278, 280–286. https://doi.org/10.1016/j.geomorph.2016.11.018.

Svensson, H., 1959. Is the Cross-Section of a Glacial Valley a Parabola? Journal of Glaciology 3, 362–363. https://doi.org/10.3189/S0022143000017032.

USGS, 2021. United States Geological Survey 3D Elevation Program 1 arc-second Digital Elevation Model. Distributed by OpenTopography. https://doi.org/10.5069/G98K778D. Accessed: 2023-08-26.

Wallick, K.N., Principato, S.M., 2020. Quantitative analyses of cirques on the Faroe Islands: evidence for time transgressive glacier occupation. Boreas 49, 828–840. https://doi.org/10.1111/bor.12458.

Wheeler, D.A., 1984. Using parabolas to describe the cross-sections of glaciated valleys. Earth Surface Processes and Landforms 9, 391–394. https://doi.org/10.1002/esp.3290090412.

Zhang, Q., Dong, W., Dou, J., Dong, G., Zech, R., 2021. Cirques of the central Tibetan Plateau: Morphology and controlling factors. Palaeogeography, Palaeoclimatology, Palaeoecology 582, 110656. https://doi.org/10.1016/j.palaeo.2021.110656.

Zhang, Q., Fu, P., Yi, C., Wang, N., Wang, Y., Capolongo, D., Zech, R., 2020. Palaeoglacial and palaeoenvironmental conditions of the Gangdise Mountains, southern Tibetan Plateau, as revealed by an ice-free cirque morphology analysis. Geomorphology 370, 107391. https://doi.org/10.1016/j.geomorph.2020.107391.